



Effects of pyrocatechol on the computational, structural, spectroscopic and thermal properties of silver-modified hydroxyapatite

Serhat Keser¹ · Aykut Yıldız² · Azeez A. Barzinjy^{3,4} · Rebaz Obaid Kareem⁵ · Bahroz Kareem Mahmood⁵ · Riyadh Saeed Agid⁶ · Tankut Ates⁷ · Mehmet Mürşit Temüz² · Suleyman Koytepe⁸ · Turan İnce⁹ · Omer Kaygili⁹ · Józef E. Sienkiewicz¹⁰ · Patryk Jasik¹⁰ · Niyazi Bulut⁹

Received: 12 February 2025 / Revised: 23 March 2025 / Accepted: 16 April 2025
© The Author(s) 2025

Abstract

This study investigates the synthesis and characterization of hydroxyapatite (HAp) ceramic biomaterials doped with silver (Ag) and pyrocatechol. HAp, commonly utilized in the treatment of hard tissues including teeth and bones, was produced and analyzed to assess the structural, morphological, elemental, and thermal properties of the materials. The phase and crystal structures of the synthesized HAp biomaterials were examined using X-ray diffraction (XRD), revealing that the incorporation of Ag and pyrocatechol influenced the crystallinity and lattice parameters. Fourier transform infrared (FT-IR) spectroscopy verified the presence of the characteristic OH- and PO₄³⁻ groups of HAp, while scanning electron microscopy (SEM) displayed consistent morphologies across all samples, free of residues or impurities. Elemental compositions were determined by energy dispersive X-ray (EDX) spectroscopy, and thermal stability was assessed through differential thermal analysis (DTA) and thermogravimetric analysis (TGA). Additionally, computational studies using density functional theory (DFT) were conducted to further investigate the electronic and structural properties of 0.44% Ag-doped HAp. The DFT calculations revealed that Ag atoms replace calcium (Ca1 and Ca2) positions in the lattice, leading to slight distortions in the lattice structure and changes in the electronic density distribution. Minor changes were observed in the band structure and electronic properties, indicating the stability and tunability of the doped system. A small amount of β-tricalcium phosphate (β-TCP) phase was also detected alongside the main HAp phase. These results underscore the importance of incorporating pyrocatechol and silver doping into HAp for biomedical applications. The resulting biomaterials exhibit enhanced structural, thermal, and electronic properties, with improved biocompatibility and antimicrobial activity.

Keywords Hydroxyapatite (HAp) · Silver (Ag) · Pyrocatechol (Pyro) · Structural characterization · Thermal properties · Density functional theory (DFT)

✉ Serhat Keser
serhatkeser@gmail.com

¹ Department of Chemical Technology, EOSB Vocational School, Firat University, Elazig 23119, Turkey

² Department of Chemistry, Faculty of Science, Firat University, Elazig 23119, Turkey

³ Department of Physics, Faculty of Science, Soran University, Kurdistan Region, Iraq

⁴ Department of Physics Education, Faculty of Education, Tishk International University, Erbil 44001, Iraq

⁵ Physics Department, College of Science, University of Halabja, Halabja 46018, Iraq

⁶ Department of Radiology Technologies, College of Health Technology, Knowledge University, Erbil 44001, Iraq

⁷ Department of Engineering Basic Sciences, Faculty of Engineering and Natural Sciences, Malatya Turgut Özal University, Battalgazi, Malatya 44210, Turkey

⁸ Department of Chemistry, Faculty of Arts & Science, Inonu University, Malatya 44280, Turkey

⁹ Department of Physics, Faculty of Science, Firat University, Elazig 23119, Turkey

¹⁰ Faculty of Applied Physics and Mathematics, Gdańsk University of Technology, Narutowicza 11/12, Gdańsk 80-952, Poland

Introduction

Biochemical materials play crucial roles in biological systems, and the field of medical inorganic compounds focuses on utilizing these materials to diagnose and treat disorders. The human body is composed of numerous chemical elements, most of which are concentrated in bones, teeth, and other organs. These elements are essential for nourishing and supporting the body's functions [1, 2]. Bioceramics are ceramic materials with biological compatibility, designed to heal and regenerate damaged tissues. These materials are essential in the field of regenerative medicine due to their ability to integrate with living tissue, promoting healing and recovery. Among the various types of bioceramics, synthetic osteoconductive bone graft materials represent the majority of ceramic biomaterials currently available for use in hard tissue replacement and healing treatments. These osteoconductive materials support the growth of new bone tissue by facilitating the attachment and proliferation of osteoblasts, which are critical for bone regeneration. Due to their excellent mechanical properties, biocompatibility, and ability to mimic the natural bone structure, synthetic bone grafts made from bioceramics have become invaluable in treating bone defects, fractures, and other skeletal system disorders [3, 4].

Hydroxyapatite (HAp) is an artificial biomaterial that is analogous to the composition of mammalian hard tissue. As a result, it is commonly used as a material for bone grafts, and as a scaffold for hard tissue engineering. HAp is a member of the apatite family and exhibits several advantageous properties, particularly in terms of its composition and characteristics. These properties include biocompatibility, antibacterial activity, flexibility, dielectric and diamagnetic behavior, osteoconductivity, biological activity, non-toxicity, as well as thermal and optical properties [5–9]. Additionally, the advancement of *in vitro* testing, a key medical application of biomaterials used in cancer research, is crucial for the biological applications of cancer treatments. This improvement also offers a more accurate understanding of pharmacological strategies and drug-delivery methods [7, 10]. It has the chemical structure of apatite: $Y_{10}(PO_4)_6 \times 2$, where Y indicates (calcium, Ca^{2+}), and X refers to (hydroxide, OH^-), with the standard formula being $Ca_{10}(PO_4)_6(OH)_2$, and Ca: P molecular ratio 1.67 [5, 6, 11, 12]. Both artificial and natural HAp crystal structure in the hexagonal form with the space group symmetry $P6_3/m$, with a structured arrangement of Ca^{2+} and $(PO_4)^{3-}$ ions around OH^- ion columns [7, 13]. These bioactive HAp materials are synthesized using various methods, including dry processes, hydrolysis, hydrothermal treatment, sol-gel processes, and wet chemical methods [7, 10, 14]. The wet approach is preferred over the dry method due to several advantages, including its higher purity, safety, cost-effectiveness, and

ease of use. Additionally, the wet process operates at lower temperatures, typically below 100 °C, making it more energy-efficient and suitable for a wider range of applications. These factors contribute to the wet method's popularity in the synthesis of bioactive materials, as it ensures better control over material properties while maintaining economic and environmental benefits [10].

To enhance the chemical and physical properties, including bonding, dielectric and diamagnetic behavior, biological activity, and mechanical characteristics of HAp and other ceramics, various anions and cations can be doped or co-doped using different additives. The common cationic species are (Mn^{2+} , Zn^{2+} , Li^{2+} , Ce^{3+} , Na^+ , Cu^{2+} , Co^{2+} , K^+ , Ag^+ , Sr^{2+} , Er^{3+} , Gd^{3+} , La^{3+} , Al^{3+} , Mg^{2+} , Yb^{3+} and etc.), along with the anionic species like (CO_3^{2-} , SiO_4^{4-} , Cl^- , and F^-) [7, 8, 15, 16]. Additionally, the cation conversion rate of HAp is quite high with heavy elements or risky ions such as Pb^{2+} , Cd^{2+} , Cu^{2+} , Mn^{2+} , Ag^+ , Co^{2+} etc., due to the interactions between complexation processes, surface adsorption, precipitation, and ion exchange [17]. Silver (Ag^+) nanoparticles exhibit unique optical properties, excellent biocompatibility, sufficient stability, as well as strong antibacterial and catalytic capabilities. These remarkable characteristics stem from their nanoscale size, which can be precisely controlled through adjustments to their physical and chemical properties. The small size of the nanoparticles enhances their reactivity, surface area, and interaction with biological systems, making them highly effective for various applications, including medical treatments, environmental remediation, and industrial catalysis [18, 19].

Ag has been shown to possess antibacterial properties, low volatility, and resistance to bacterial infections. It also exhibits thermal stability, is non-toxic to human cells at low doses, and maintains minimal cytotoxicity [9, 12, 14, 19, 20]. It has been established that increasing the Ag content in the material enhances its antibacterial effects, but this also leads to a rise in cytotoxicity. Cytotoxicity refers to the ability of a material or process to damage or kill cells [21]. It has been found that a high concentration of Ag^+ ions > 1.6 ppm, is cytotoxic, impacting the fundamental metabolic cellular activities of mammalian cells [22]. Ag^+ ions are absorbed from the solution and transferred into the Ca^{2+} site of HAp based on the apatite structure's capacity for ion exchange [22]. Substituting the greater ionic radius (1.28 Å) of Ag^+ with the shorter ionic radius (0.99 Å) of Ca^{2+} in the HAp lattice allows stress and strain in the crystal structure [12].

Based on the findings of Jacobs et al. [23], Ag-doped HAp demonstrates significant bactericidal efficacy and exhibits a notable release rate and kinetics within the human body. Research has shown that materials combining the antibacterial properties of silver with the bioactivity, biocompatibility, and osteoconductivity of HAp create a substance that

is both biocompatible and effective against bacterial infections [24–27]. The literatures indicate that Ag/HAp exhibits potent antibacterial activity against both gram-negative and gram-positive bacteria, with its efficacy strongly dependent on the concentration of Ag ions incorporated [17, 22, 27, 28]. Many studies have proven that physical, chemical and biological characteristics of HAp samples are positively affected when they are doped with Ag [29–31]. There are also studies showing that the corrosion resistance and biocompatibility of Ag-doped HAp samples increase with Ag doping [32, 33].

Pyrocatechol, a chemical compound with the molecular formula $C_6H_4(OH)_2$, is also known as catechol or 1,2-dihydroxybenzene. It exhibits both prooxidant and antioxidant properties. Potential therapeutic applications of pyrocatechol have been explored in various areas, including neuroprotection, anti-inflammatory effects, and cancer prevention. Additionally, pyrocatechol serves as a model compound for

lignin in plants and aromatic substances found in wastewater [34]. The antioxidant effects of pyrocatechol stem from its ability to scavenge free radicals and reactive oxygen species, a property that is likely related to its chemical characteristics [35]. Pyrocatechol is capable of undergoing a wide range of reactions, including complex formation and redox processes [36]. It can interact with metal ions to form complexes and participate in electron transfer reactions. Additionally, pyrocatechol can be enzymatically produced with peroxidase as a catalyst in aqueous dioxane solutions or reverse micellar systems [36].

Recent studies suggest that the incorporation of pyrocatechol into silver-doped hydroxyapatite (Ag-HAp) plays three key roles: modulation of its spectroscopic properties, enhancement of its electrochemical sensing performance and possible enhancement of its antibacterial efficacy through synergistic interactions with the doped silver ions. The presence of silver doping appears to impart distinct characteristics to pyrocatechol-containing materials, affecting their structural and functional properties.

This study investigates the effect of pyrocatechol content on the synthesis of Ag-doped hydroxyapatite (Ag-HAp), with particular emphasis on its structural, thermal and spectroscopic properties. The incorporation of pyrocatechol induces significant shifts in characteristic vibrational bands, particularly in the hydroxyl (OH^-) and phosphate (PO_4^{3-}) stretching regions. These spectral variations will be analysed using FT-IR spectroscopy to confirm the molecular level interactions between pyrocatechol and Ag-HAp.

Materials and methods

Synthesis

Hydroxyapatite (HAp) samples were synthesized using a wet chemical method with high-purity precursors: calcium nitrate tetrahydrate ($Ca(NO_3)_2 \cdot 4H_2O$), silver nitrate ($AgNO_3$), diammonium hydrogen phosphate ($(NH_4)_2HPO_4$, DAP), and pyrocatechol, all sourced from Sigma-Aldrich. The synthesis was carried out with an atomic calcium (Ca) content of 99.56% and an atomic silver (Ag) content of 0.44%. The synthesis process is given in a flowchart in Fig. 1.

During the synthesis, varying volumes (0, 5, 10, and 15 mL) of 0.05 M pyrocatechol solution were introduced into the reaction mixture to investigate its effects on the final material properties. The required amount of pyrocatechol was first dissolved in deionized water to ensure homogeneity.

The synthesis process began with dissolving the appropriate amount of DAP in deionized water using a volumetric

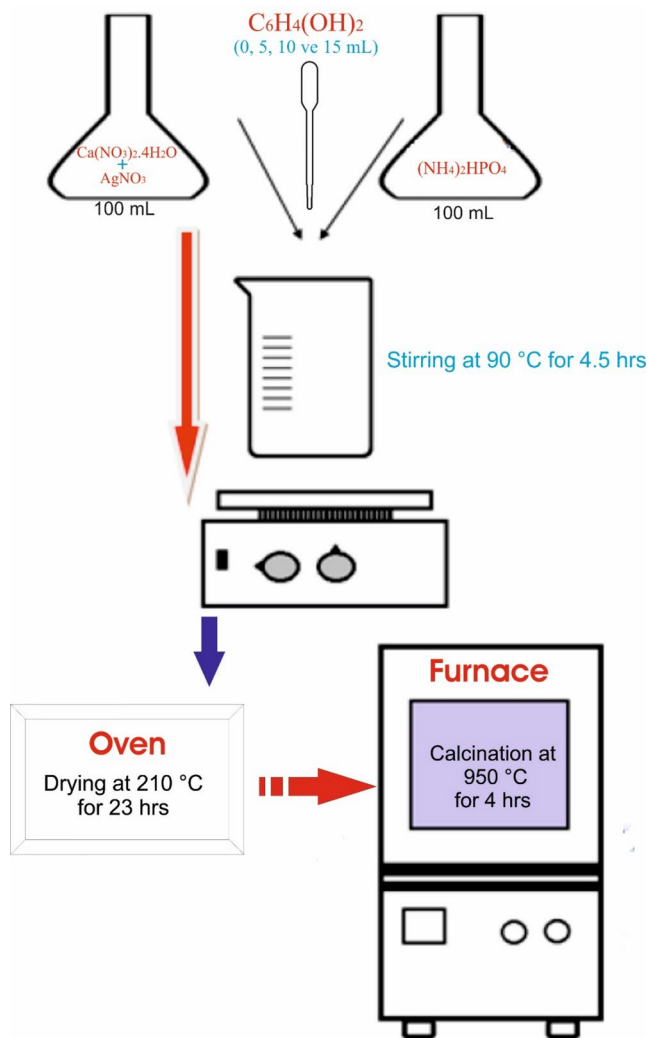


Fig. 1 Flowchart of the synthesis steps of the samples

flask. Separately, $\text{Ca}(\text{NO}_3)_2 \cdot 4\text{H}_2\text{O}$ and AgNO_3 were dissolved in deionized water in another volumetric flask. The resulting calcium-silver solution was then added dropwise to the DAP solution while continuously stirring on a heated magnetic stirrer. Subsequently, the designated volume of pyrocatechol was introduced dropwise into the final reaction mixture.

The resulting mixture was stirred at 90 °C for 4.5 h until a gel-like consistency was achieved. Following this, the samples were dried in an oven at 210 °C for 23 h to remove residual moisture. The dried materials were then transferred to porcelain crucibles and subjected to calcination in a muffle furnace at 950 °C for 4 h. This process yielded HAp samples in the form of white powder.

The synthesized samples were designated as P1, P2, P3, and P4, corresponding to the increasing concentrations of pyrocatechol incorporated during synthesis.

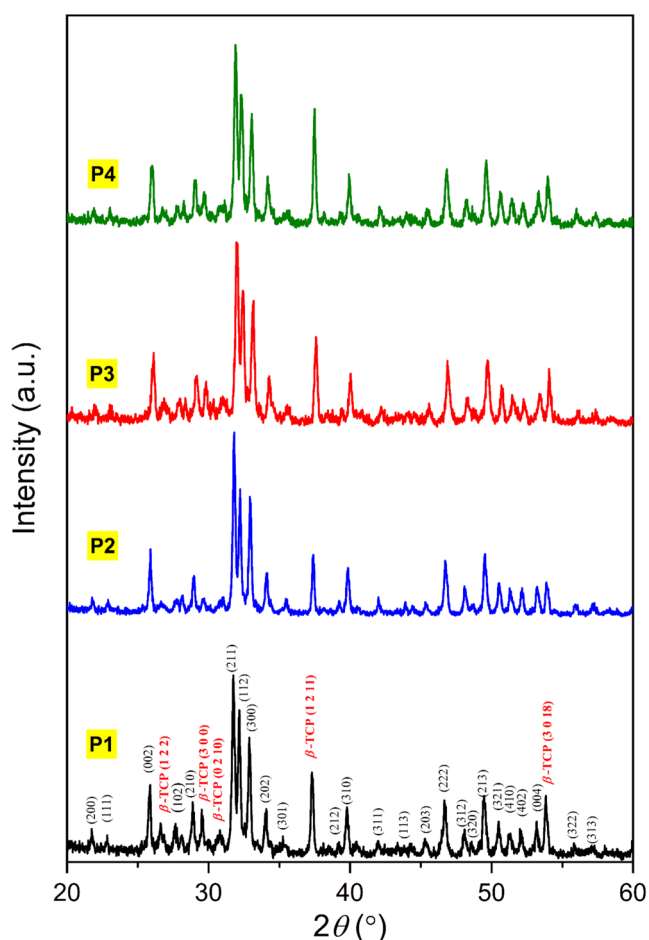


Fig. 2 XRD plots of the as-produced HApS

Characterization

The structural, morphological, elemental, and thermal properties of the synthesized hydroxyapatite (HAp) samples were characterized using various analytical techniques.

X-ray diffraction (XRD)

The crystalline structure of the HAp samples was analyzed using X-ray diffraction (XRD) with $\text{CuK}\alpha$ radiation ($\lambda=0.15406$ nm) on a Rigaku RadB-Dmax II diffractometer operating at 40 kV and 40 mA in the 2θ range from 20° to 60° using the steps of 0.02°.

Fourier transform infrared (FT-IR) spectroscopy

Functional group analysis was performed using Fourier transform infrared (FT-IR) spectroscopy on a PerkinElmer Spectrum One spectrometer within the spectral range of 400–4000 cm^{-1} . The KBr pellet technique was employed to prepare the samples for analysis.

Scanning electron microscopy (SEM) and energy dispersive X-ray (EDX) spectroscopy

The surface morphology of the synthesized HAp samples was examined using a Zeiss EVO-MA10 scanning electron microscope (SEM). The elemental composition of selected regions was determined using an energy dispersive X-ray (EDX) Bruker XFlash detector.

Thermal analysis (DTA/TGA)

The thermal stability and decomposition behavior of the synthesized HAp biomaterials were evaluated using differential thermal analysis (DTA) and thermogravimetric analysis (TGA). These measurements were conducted on Shimadzu DTA-50 and TGA-50 instruments, respectively. For both analyses, the min^{-1} . The DTA and TGA measurements were performed from room temperature to 900 °C with a heating rate was 10 °C.

Results and discussion

Experimental results

XRD analysis

The X-ray diffraction (XRD) analysis results of the synthesized hydroxyapatite (HAp) samples are presented in Fig. 2. In all samples, the dominant crystalline phase was identified

as HAp, corresponding to the standard reference pattern (JCPDS PDF No: 09-0432), while the secondary phase was detected as β -tricalcium phosphate (β -TCP), matching the reference pattern (JCPDS PDF No: 09-0169).

A detailed examination of the diffraction patterns reveals the influence of both pyrocatechol and silver (Ag) doping on phase composition and crystallinity. The incorporation of Ag and pyrocatechol appears to induce subtle changes in peak intensities and shifts, suggesting modifications in lattice parameters and crystallinity percentages. These alterations may be attributed to ionic substitution, structural distortions, or interactions between the dopants and the HAp matrix.

Furthermore, the presence of the β -TCP phase, albeit in minor quantities, indicates partial decomposition or phase transformation, which could be influenced by the dopant concentrations and synthesis conditions. Notable, even sample P1, which contains 0% pyrocatechol, shows traces of β -TCP. This suggests that the formation of β -TCP is not solely dependent on the incorporation of pyrocatechol, but may result from inherent factors such as precursor selection, synthesis parameters and thermal treatment.

From Fig. 2, the XRD analysis confirms the presence of the β -TCP phase in sample P1, suggesting that phase transformation may have occurred due to the calcination temperature (950 °C). At high temperatures, hydroxyapatite (HAp) can undergo thermal decomposition into β -TCP, especially under conditions of slight calcium deficiency or non-stoichiometric synthesis. In addition, the possible volatilisation of hydroxyl (OH⁻) groups during high temperature processing may contribute to this phase transition. These results are consistent with previous reports [37, 38] that β -TCP formation can result from factors such as prolonged heating times, partial dehydroxylation of HAp and variations in the Ca/P ratio. Therefore, the observed β -TCP in sample P1 may be an intrinsic consequence of the synthesis and calcination

process rather than an effect of pyrocatechol incorporation alone.

The crystallite size (D) of all samples was calculated by the Scherrer equation [39]:

$$D = \frac{0.9\lambda}{\beta \cos\theta} \quad (1)$$

In Eq. (1), β represents the maximum half peak width; λ represents the X-ray wavelength; θ represents the Bragg angle. The D value for the diffraction patterns of the samples was calculated separately as D_{002} and D_{300} for the (002) and (300) planes, respectively, and the obtained values are shown in Table 1.

Both the lattice parameters (a and c) and the unit cell volume (V) were calculated using the following equations, respectively [39].

$$\frac{1}{d^2} = \frac{4}{3} \left(\frac{h^2 + hk + k^2}{a^2} \right) + \frac{l^2}{c^2} \quad (2)$$

$$V = 0.866a^2c \quad (3)$$

In the above equations, the letters h , k and l represent Miller indices.

The crystallization percentages ($X_C\%$) of the samples were determined using the following equation, as reported by Landi et al. [40]:

$$X_C\% = \left(1 - \frac{V_{112/300}}{I_{300}} \right) \times 100 \quad (4)$$

In this equation, $V_{112/300}$ represents the intensity of the trough between the (112) and (300) reflections, and I_{300} represents the intensity of the reflection belonging to the (300) plane [41]. All the parameters calculated by the analysis of XRD data and mentioned above are presented in Table 1.

Table 1 The calculated values related to the XRD analysis

		P1	P2	P3	P4
<i>Experimental results</i>	<i>HAp phase (%)</i>	86.0	85.8	87.1	87.0
	<i>β-TCP phase (%)</i>	14.0	14.2	12.9	13.0
	<i>$X_C\%$</i>	80.2	84.5	77.7	81.3
	<i>D (nm)</i>	40.63	45.76	33.13	36.37
	<i>a (nm)</i>	0.9423	0.9412	0.9351	0.9384
	<i>c (nm)</i>	0.6885	0.6875	0.6818	0.6843
	<i>V (nm)³</i>	0.5294	0.5274	0.5163	0.5218
<i>Theoretical results</i>	<i>For Ca1 site</i>	<i>a (nm)</i>	0.9469		
		<i>c (nm)</i>	0.6790		
		<i>V (nm)³</i>	0.5272		
	<i>For Ca2 site</i>	<i>a (nm)</i>	0.9402		
		<i>c (nm)</i>	0.6827		
		<i>V (nm)³</i>	0.5226		

An analysis of the data presented in Table 1 reveals that the incorporation of both pyrocatechol and silver (Ag) significantly influences the structural parameters of the synthesized hydroxyapatite (HAp) samples. The lattice parameters (a and c) exhibit notable variations, suggesting that the dopants induce structural modifications within the HAp lattice. The crystallinity percentages of the samples range between 77.7% and 84.5%, indicating that the degree of crystallization is influenced by the presence of Ag and pyrocatechol. The degree of crystallization in the synthesized samples is influenced by both Ag doping and pyrocatechol incorporation. However, in sample P1, which lacks pyrocatechol, the observed crystallization behavior is primarily attributed to the influence of Ag doping and synthesis conditions. The variation in crystallinity across all samples suggests that Ag incorporation alone can modify the structural properties of hydroxyapatite by inducing lattice distortions and affecting nucleation kinetics. Furthermore, in samples containing pyrocatechol (P2–P4), additional interactions with the hydroxyapatite lattice may contribute to further changes in crystallinity. The structural changes induced by pyrocatechol could result from coordination interactions, surface adsorption or molecular level bonding effects, leading to variations in lattice parameters and crystallinity percentages. The comparative analysis of P1 (Ag-doped HAp without pyrocatechol) and the other samples (Ag-HAp with pyrocatechol) supports the conclusion that while Ag doping alone influences crystallinity, the combined presence of Ag and pyrocatechol introduces additional structural effects.

The relative phase composition of the samples further demonstrates the impact of these dopants. The HAp phase percentages follow the order: P3 (87.1%) > P4 (87.0%) > P1 (86.0%) > P2 (85.8%), while the β -TCP phase percentages are reported as P1 (14.2%) > P2 (14.0%) > P4 (13.0%) > P3 (12.9%).

The β -TCP phase percentage was determined using X-ray diffraction (XRD) analysis by evaluating the relative intensities of specific diffraction peaks corresponding to β -TCP and hydroxyapatite (HAp) phases. The primary peak used for β -TCP quantification is the (0210) reflection, located around $2\theta \approx 31.0$ – 31.2° , as identified in the standard JCPDS reference pattern (JCPDS PDF No: 09-0169). The phase fraction was calculated using the intensity ratio method, where the proportion of β -TCP in each sample was estimated relative to the sum of major HAp and β -TCP peaks.

These results suggest that the phase stability and distribution are dependent on the specific doping conditions employed during synthesis.

A comparison with literature data supports these findings. Kaygili et al. [42] reported that the crystallization percentages of Ag-doped HAp samples ranged from 88.3 to 90.2%, with the HAp phase varying between 94.7% and 96.9%, and

the β -TCP phase constituting 3.1–5.3%. Similarly, Aqib et al. [43] demonstrated that Ag⁺ doping influences the crystallographic parameters of brushite samples, as confirmed by XRD analysis.

Further studies have also investigated the variations in lattice parameters due to Ag incorporation. Makarova et al. [44] reported that the lattice parameters of Ag-doped HAp samples varied within the range of $a \approx 0.94371$ – 0.94673 nm and $c \approx 0.68912$ – 0.69124 nm, highlighting the structural modifications induced by Ag doping. Additionally, Sahin et al. [45] demonstrated that doping HAp with Ag, Pr, and Zn significantly affects crystallinity, crystallite size, lattice parameters, and unit cell volume, further supporting the present findings.

Adhitiyan et al. [46] determined that Ag-doped HAp samples produced by green synthesis using the microwave method had functional and structural HAp characteristics as a result of FTIR and XRD analyses.

Moreover, Hossain et al. [47] determined that the crystallite size of HAp samples doped with 0.25%, 0.5%, 1.0%, and 2.5% Ag ranged from $D \approx 75.2$ – 91.2 nm, with HAp phase content varying between 52.49% and 85.53%, and β -TCP phase content ranging from 15.47 to 47.51%. The reported lattice parameters for these Ag-doped HAp samples fell within $a \approx 0.93794$ – 0.94594 nm and $c \approx 0.68362$ – 0.68796 nm. Similarly, Mendez-Lozano et al. [48] found that the crystallite size of Ag-doped HAp samples ranged from $D \approx 47.51$ – 48.34 nm, with lattice parameters between $a \approx 0.921$ – 0.925 nm and $c \approx 0.677$ – 0.679 nm.

These comparative studies emphasize that Ag and pyrocatechol doping induce measurable changes in the crystallographic properties of HAp, affecting its structural stability and phase composition. The observed variations in lattice parameters, crystallinity, and phase distribution highlight the tunability of Ag-doped HAp for potential biomedical applications.

FT-IR analyses

The FT-IR spectra of 0.44% Ag-doped hydroxyapatite (HAp) samples containing varying concentrations of pyrocatechol (0, 5, 10, and 15 mL) are depicted in Fig. 3. The characteristic vibrational bands corresponding to the phosphate (PO_4^{3-}) group were observed at 473, 565, 600, 962, 1031, and 1089 cm^{-1} for all samples (P1, P2, P3, and P4) [41, 49]. These bands are indicative of the fundamental structural units of the hydroxyapatite lattice.

The presence of the hydroxyl (OH^-) group was confirmed by distinct absorption bands at 630 and 3642 cm^{-1} , which are characteristic of the stretching and librational vibrations of OH^- ions in HAp [50]. Additionally, the characteristic absorption bands corresponding to the carbonate (CO_3^{2-})

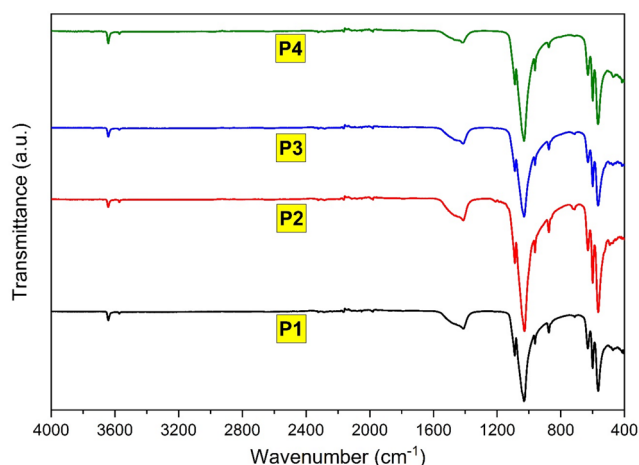


Fig. 3 FTIR spectra of the as-prepared HAPs

group were detected at 875, 1412, and 1463 cm^{-1} for all samples, suggesting partial carbonate substitution within the HAP structure, likely due to atmospheric CO_2 incorporation during synthesis [51].

A comparative analysis with existing literature highlights consistent findings in Ag-doped HAP and other calcium phosphate (CaP) compounds. Aqib et al. [43] reported characteristic vibrational modes for CaP compounds, including PO-bending at 573 cm^{-1} , P–O(H) stretching at 872 cm^{-1} , PO-stretching at 980 and 1225 cm^{-1} , H_2O bending at 1652 cm^{-1} , and O–H stretching at 3540 cm^{-1} , in Ag⁺-doped brushite samples.

Similarly, Makarova et al. [44] identified O–P–O bending vibrations at 572 and 602 cm^{-1} , P–O stretching vibrations at 960, 1048, and 1091 cm^{-1} , OH^- oscillation at 630 cm^{-1} , and OH^- stretching at 3571 cm^{-1} in Ag-doped HAP samples (0.2, 0.5, 1.0, 1.5, and 2.0 mol Ag). Their study also detected absorption bands at 876, 1418, and 1472 cm^{-1} , attributed to carbonate ions formed due to direct CO_2 capture from ambient air, reinforcing the findings of the present study.

Moreover, Mendez-Lozano et al. in 2023 [48] demonstrated that 0.05, 0.1, and 0.2 mol Ag-doped HAP samples retained the characteristic FT-IR peaks of the HAP structure, indicating that Ag incorporation does not significantly alter the fundamental vibrational properties of the material. Rajan et al. in 2024 [52] further confirmed the presence of phosphate groups (PO_4^{3-}) in Ag-doped HAP samples and identified hydroxyl groups at 3569 and 631 cm^{-1} and carbonate species at 1410, 870, and 1460 cm^{-1} . Their study concluded that these absorption bands represent the fundamental structure of HAP and that Ag doping does not induce structural disruptions in the HAP lattice.

Taken together, these results indicate that Ag doping in conjunction with pyrocatechol does not significantly alter the fundamental spectral features of hydroxyapatite (HAP), as confirmed by the retention of characteristic phosphate

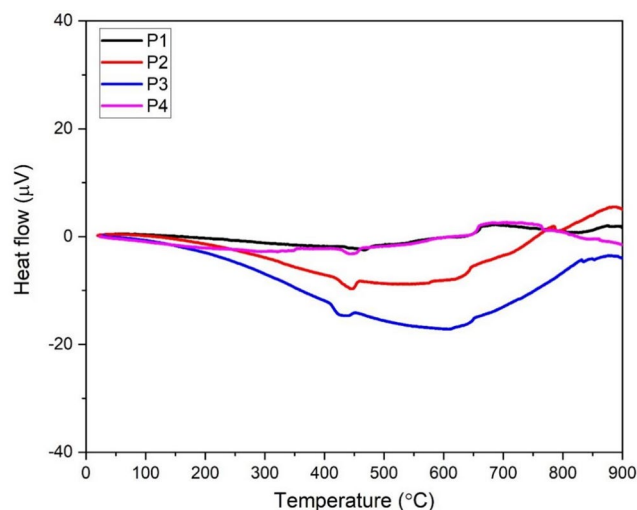


Fig. 4 DTA plots of the pyrocatechol containing HAPs

(PO_4^{3-}) and hydroxyl (OH^-) vibrational bands in the FT-IR spectra. However, the incorporation of Ag and pyrocatechol may introduce additional functionalities through antibacterial activity and improved biocompatibility. Ag⁺ ions are well documented to have strong antimicrobial properties, mainly through their interaction with bacterial cell membranes, generation of reactive oxygen species (ROS) and disruption of DNA replication pathways [17, 27]. In addition, the incorporation of Ag into HAP has been shown to enhance osteoblast adhesion and proliferation, thereby improving biocompatibility in biomedical applications [21, 22]. Furthermore, pyrocatechol is known for its redox activity and metal chelating properties, which may contribute to improved biological performance by stabilising Ag⁺ ions and modulating surface interactions with biological systems [35]. Previous studies have shown that catechol-containing compounds can enhance bioactivity, antimicrobial efficacy and tissue integration in composite biomaterials [53].

Therefore, while Ag and pyrocatechol do not induce major structural perturbations in HAP, their presence potentially enhances functional properties, including antibacterial activity and biocompatibility, making the material a promising candidate for bone grafts, dental coatings and antimicrobial surfaces.

Thermal analysis

The Differential Thermal Analysis (DTA) curves, recorded over a temperature range from room temperature to 1000 °C, as depicted in Fig. 4, indicate that all the synthesized samples exhibit thermal stability within this interval [54, 55]. However, as shown in Fig. 5, mass losses are observed for all samples within the same temperature range. Specifically, the mass losses are quantified as 4.96%, 3.60%, 3.10%,

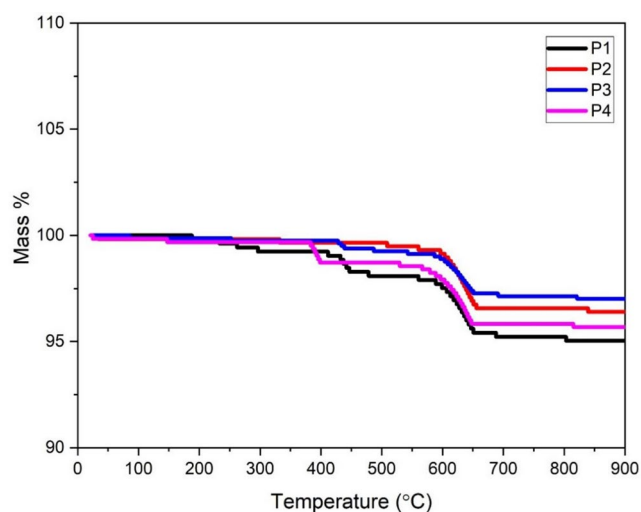


Fig. 5 TGA graphs of the pyrocatechol containing HAp samples

and 4.48% for samples P1, P2, P3, and P4, respectively. The observed variations in mass loss suggest that both Ag and pyrocatechol influence thermal stability. Pyrocatechol incorporation appears to increase resistance to degradation (P2, P3), while higher pyrocatechol content (P4) results in additional mass loss due to organic degradation. These results suggest a potential synergistic effect between Ag and pyrocatechol, which could be beneficial in the design of thermally stable biomaterials for biomedical applications. The thermal degradation occurring between 200 °C and 600 °C is attributed primarily to dehydroxylation and the elimination of lattice water, which is consistent with findings reported in previous studies [56, 57].

A review of the existing literature reveals that while hydroxyapatite (HAp) biomaterials doped with silver (Ag) and pyrocatechol have been synthesized separately, no studies have reported the fabrication of HAp materials co-doped with both Ag and pyrocatechol. In the context of related investigations, Lima et al. [53] demonstrated that catechol-derived polymers facilitate mineral deposition on demineralized dentin surfaces, highlighting their potential in dental applications. Similarly, Kaygili et al. [58] reported that Ag/Gd-doped HAp samples possess high thermal stability and favorable dielectric properties, suggesting their applicability in bone regeneration. The antimicrobial and bone regenerative potential of Ag and pyrocatechol doped hydroxyapatite (HAp) is based on the well-documented biological effects of its individual components. Silver (Ag) is widely recognized for its antibacterial properties, as it disrupts bacterial cell membranes, interferes with DNA replication and generates reactive oxygen species (ROS), making it effective against a wide range of pathogens [17, 27]. Pyrocatechol, a phenolic compound, has been shown to enhance redox activity and bio functionality, potentially

contributing to antibacterial effects and osteoblast adhesion [53]. In addition, hydroxyapatite itself is a well-established biomaterial for bone regeneration due to its chemical similarity to natural bone mineral and its ability to promote cell attachment and proliferation [59]. Although no direct in vitro antibacterial or osteogenic assays were performed in this study, the observed structural stability, controlled Ag incorporation and presence of bioactive functional groups suggest potential applications in biomedical coatings and bone repair materials. Future work will focus on evaluating cytotoxicity, osteoblast response and bacterial inhibition assays to confirm these effects experimentally.

Furthermore, Makarova et al. [44] investigated the thermal behavior of Ag-doped HAp samples and found that increasing silver substitution levels (0.2, 0.5, 1.0, 1.5, and 2.0 mol) led to a progressive decline in thermal stability. These findings underscore the necessity of further research to assess the structural, thermal, and functional implications of co-doping HAp with Ag and pyrocatechol, which could open new avenues for biomedical applications.

SEM and EDX analysis

Figure 6 presents the scanning electron microscope (SEM) images of all synthesized samples alongside the corresponding energy-dispersive X-ray (EDX) spectra obtained from the analyzed regions. Examination of these spectra and micrographs confirms the successful incorporation of the intended dopant elements in each sample, with no detectable impurities. Morphological analysis further reveals that all samples exhibit a granular structure, characterized by small, closely packed grains with interspersed pores, indicative of a porous microstructure.

Quantitative elemental analysis based on EDX measurements yields (Ca+Ag)/P molar ratios of 3.555, 2.177, 2.013, and 1.484 for samples P1, P2, P3, and P4, respectively. These values deviate from the stoichiometric ratio of 1.67, which is characteristic of pure hydroxyapatite (HAp), thereby confirming the presence of a calcium-deficient HAp phase [40, 41]. The observed Ca deficiency could influence the physicochemical properties of the material, potentially affecting its bioactivity, dissolution behavior, and structural integrity. Such deviations from stoichiometry are commonly reported in doped HAp systems and are known to play a crucial role in tailoring the material's performance for biomedical applications. EDX analysis primarily confirms the incorporation of silver (Ag) in Ag-HAp samples. However, due to its organic nature, pyrocatechol cannot be directly identified by EDX. While an increase in carbon content may indicate the presence of pyrocatechol, such results must be interpreted with caution as carbon contamination from the environment or sample preparation may also contribute

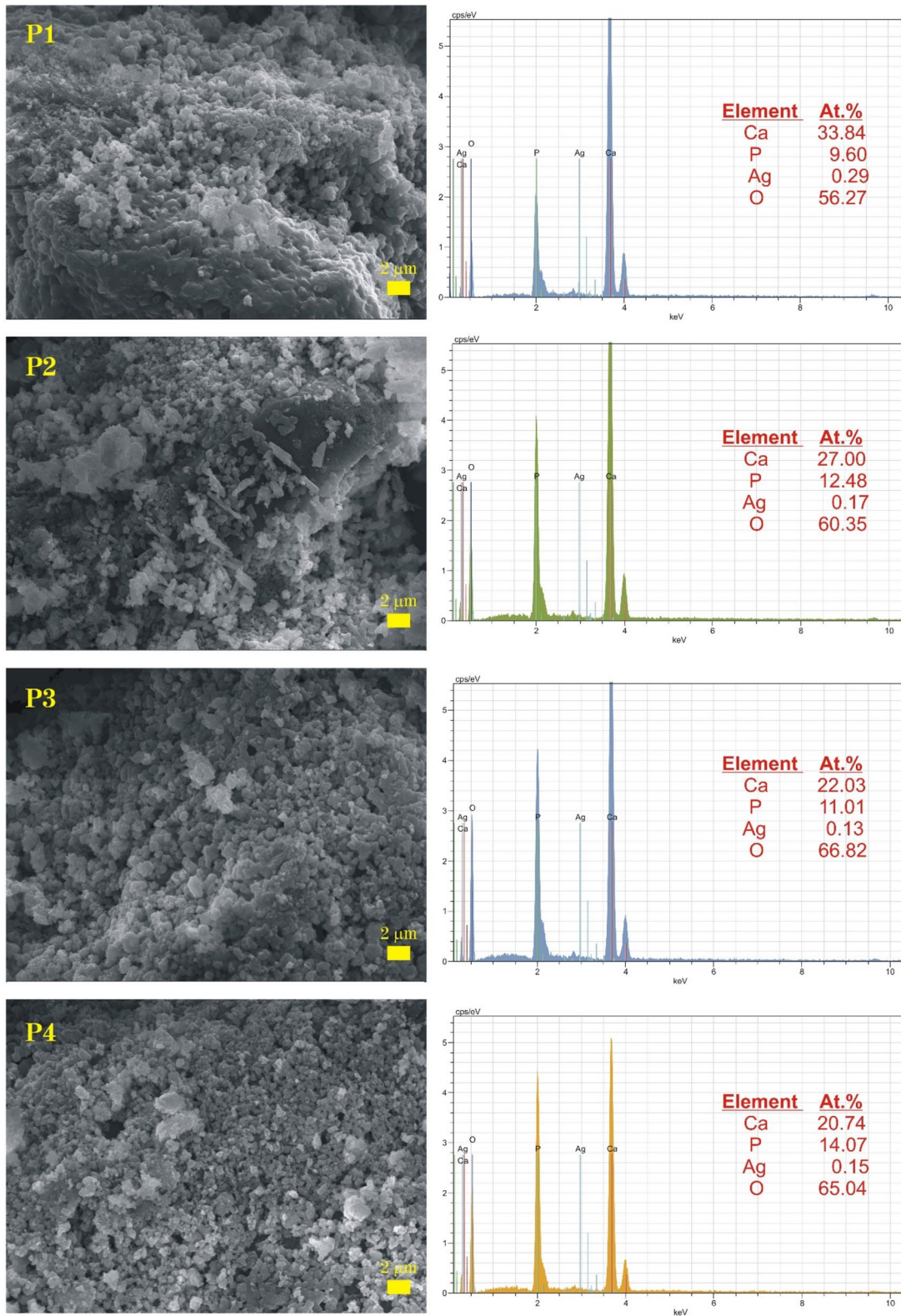


Fig. 6 Morphological investigation of the samples using SEM and EDX techniques

to the signal. FT-IR spectroscopy was used to validate the incorporation of pyrocatechol, showing distinct absorption bands associated with hydroxyl (-OH) and aromatic C=C vibrations. In addition, thermogravimetric analysis (TGA) provided evidence of pyrocatechol decomposition, further confirming its presence in the Ag-HAp system.

Further investigations, including phase analysis and in-depth structural characterization, would be beneficial to elucidate the implications of this compositional variation on the thermal stability and functional properties of the synthesized materials.

Theoretical results

In this study, density functional theory (DFT) was used to investigate the structural and electronic properties of hydroxyapatite (HAp) doped with 0.44% silver (Ag), where Ag atoms replace the calcium (Ca1 and Ca2) positions in the lattice and due to its similar ionic radius makes slight lattice distortions as shown in Fig. 7. The lattice parameters for the Ca2 site were determined to be $a=b=0.9402$ nm and $c=0.6827$ nm with a cell volume of 0.5226 nm³, while for the Ca1 site the parameters were $a=b=0.9469$ nm, and $c=0.6790$ nm with a cell volume of 0.5272 nm³. Both structures retained hexagonal symmetry with a space group of P6₃/m and point group symmetry of C6_h, indicating only minor lattice distortions upon Ag doping. These small structural changes are attributed to the larger ionic radius and higher electronegativity of Ag compared to Ca, which slightly redistribute the electron density within the lattice.

The system was treated as metallic during the electronic minimization process, employing density mixing techniques with Gaussian smearing to optimize the electron density distribution. The theoretical framework and computational methodology have been detailed in our previous works [37, 38]; however, a brief explanation is provided here.

To ensure an accurate representation of the electronic wave functions and potential energy surfaces, a smearing

width of 0.1 eV was applied, and a plane wave basis set cut-off of 700 eV was used. The electronic structure calculations were performed using the Perdew-Burke-Ernzerhof (PBE) exchange-correlation functional within the framework of the Generalized Gradient Approximation (GGA), which offers a balance between computational efficiency and accuracy. This approach provides a reliable description of the system's electronic properties while maintaining computational feasibility.

The convergence criteria were strictly enforced, with the total energy per atom and the eigenenergies converging to 0.2×10^{-5} eV and 0.46×10^{-6} eV, respectively. A Monkhorst-Pack lattice with $2 \times 2 \times 4$ k-point sampling was used for Brillouin zone integration, effectively capturing the periodicity and electronic interactions in the lattice and. The Generalized Gradient Approximation (GGA-PBE) functional was used for the exchange-correlation interactions, with ultrasoft pseudopotentials (USP) to describe the nuclear-valence interactions. The band structure and density of states (DOS) calculations, as presented in Fig. 7, reveal subtle modifications to the electronic band edges, indicative of changes in the electronic density distribution that may influence the bandgap of the material. Specifically, Ag doping reduces the bandgap from 4.011 eV for the Ca1 site to 3.763 eV for the Ca2 site, as illustrated in Fig. 8. This bandgap reduction, along with the emergence of localized states near the conduction band edge, is expected to enhance redox activity and contribute to the antimicrobial efficacy of the material.

Furthermore, the system retained all 12 symmetry operations in the absence of ionic constraints or external pressure, confirming its structural stability upon Ag incorporation. The observed electronic and structural modifications suggest that Ag doping facilitates electron delocalization, which may enhance the electrical conductivity of the material while introducing redox-active centers. These characteristics are particularly relevant for biomedical applications, where the bioactivity of silver can improve antimicrobial

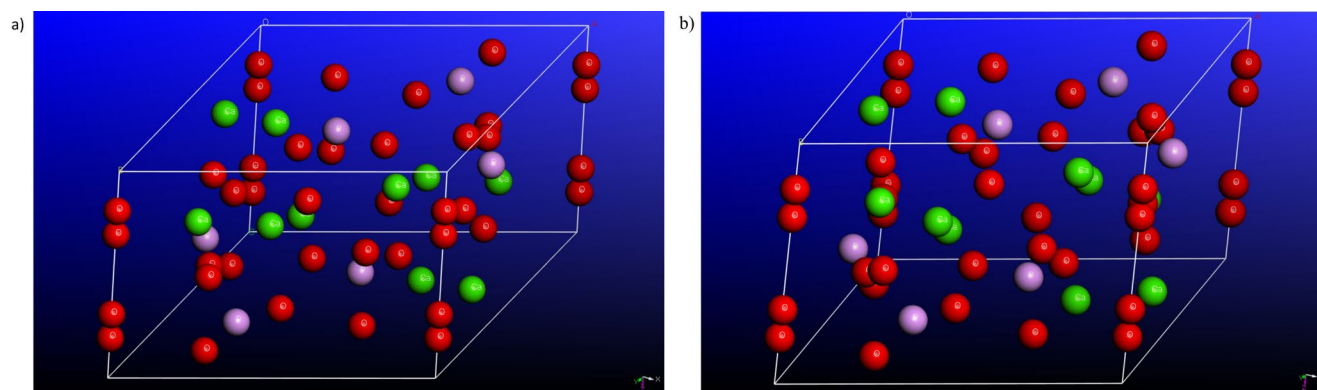


Fig. 7 Geometry structure for: (a) Ag occupying the Ca1 site, (b) Ag occupying the Ca2 site. Color legend: Red: Oxygen, Green: Calcium, Purple: Phosphorus

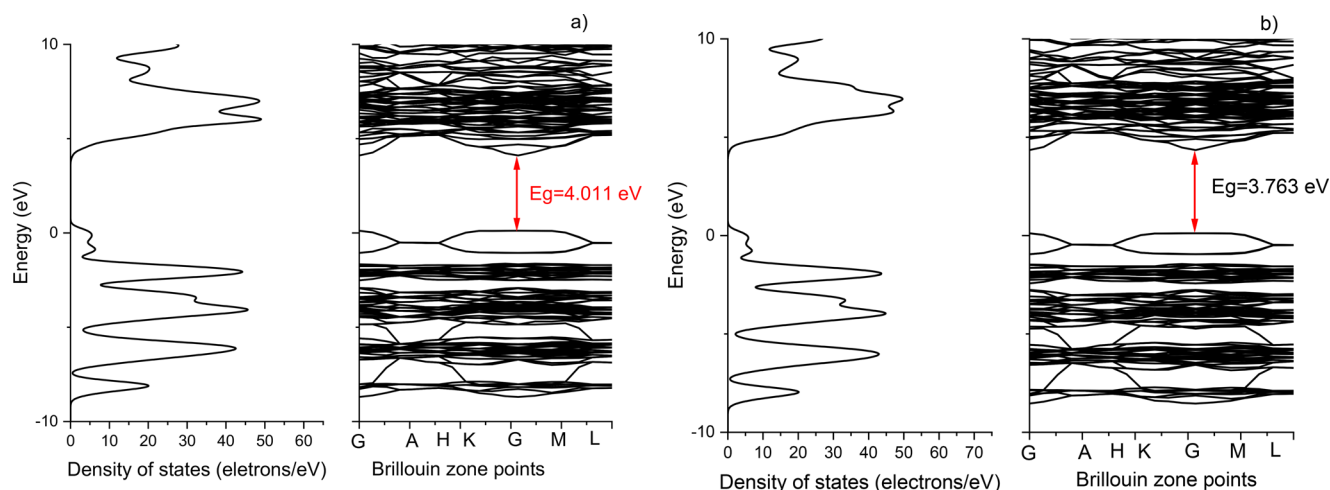


Fig. 8 Density of states and band structure (a) for Ca1 site (b) Ca2 site

performance, and for catalytic applications, where redox-active sites can promote oxidation-reduction reactions.

The ability to modulate the structural and electronic properties through Ag doping underscores the versatility of this modified HAp system. The minor lattice distortions and band structure adjustments observed in this study suggest that Ag-doped HAp holds significant promise as a multifunctional material for advanced technological applications, including biomedical implants, antimicrobial coatings, and catalysis.

The DFT calculations provide insight into the structural and electronic effects of Ag substitution at the Ca sites in hydroxyapatite (HAp). The computational results predict small lattice distortions upon Ag incorporation, which should be reflected in the experimental XRD and FTIR data. The DFT predictions are in good agreement with the XRD and FTIR experimental results, confirming that the Ag incorporation induces only minor structural changes while preserving the hexagonal HAp framework. The slight band-gap reduction predicted by the DFT calculations suggests a potential improvement in charge transport properties, which should be further validated in future electrical and dielectric studies.

Conclusions

In this study, hydroxyapatite (HAp) biomaterials co-doped with pyrocatechol and silver (Ag) were successfully synthesized using a wet chemical method. Their crystal structures, elemental compositions, functional groups, and morphologies were comprehensively analyzed. The findings demonstrate that the dual-doping approach is an effective strategy for enhancing the bioactivity and biocompatibility of HAp

while maintaining cost efficiency, making it a promising candidate for biomedical applications.

The synergistic effects of pyrocatechol and Ag doping were found to significantly influence the lattice parameters and crystallinity of the HAp samples, as confirmed by both experimental characterization and computational analyses. Structural investigations, including SEM and EDX, revealed that the synthesized HAp biomaterials exhibited homogeneous morphologies and were free from impurities or undesired residues, further confirming the effectiveness of the synthesis process.

Complementary density functional theory (DFT) calculations provided additional insights into the electronic and structural modifications induced by Ag doping. The substitution of Ca1 and Ca2 sites by Ag atoms led to slight lattice distortions and changes in the electronic band structure, thereby introducing tunable properties that could be leveraged for specific biomedical and technological applications. Notably, the doped HAp systems retained their structural integrity while exhibiting improved electronic characteristics, which may enhance their performance in various functional roles.

Overall, this study highlights the feasibility of synthesizing pyrocatechol- and Ag-doped HAp as cost-effective, biocompatible biomaterials with enhanced structural and electronic properties. These findings suggest that such modified HAp systems hold significant potential for biomedical applications, including bone regeneration, dental treatments, wound healing, biomarker detection, and targeted drug delivery. Future research should focus on in vivo biocompatibility assessments and further optimization of the doping strategy to expand the applicability of these materials in clinical settings.

Author contributions Serhat Keser: Conceptualization, Methodology, Investigation, Formal analysis, Writing-Original Draft, Supervision,

Project administration, Resources, Funding acquisition. Aykut Yildiz: Investigation. Azeez A. Barzinjy: Writing-Review & Editing, Investigation, Formal analysis. Rebaz Obaid Kareem: Writing-Original Draft, Investigation, Methodology. Bahroz Kareem Mahmood: Investigation, Methodology. Riyadh Saeed Agid: Investigation, Methodology. Tankut Ates: Investigation, Methodology, Resources, Formal analysis. Mehmet Mürşit Temüz: Investigation. Suleyman Koytepe: Investigation. Turan Ince: Methodology, Investigation, Formal analysis. Omer Kaygili: Writing-Original Draft, Methodology, Resources, Investigation, Formal analysis, Writing- Reviewing and Editing. Józef E. Sienkiewicz: Data Curation, Methodology, Investigation, Software, Formal analysis. Patryk Jasik: Data Curation, Methodology, Investigation, Software, Formal analysis. Niyazi Bulut: Data Curation, Methodology, Investigation, Software, Formal analysis.

Funding Open access funding provided by the Scientific and Technological Research Council of Türkiye (TÜBİTAK).

This work was supported by the Management Unit of Scientific Research Projects of Firat University (FUBAP) (Project Numbers: MMY.22.02 and ADEP.24.01).

Data availability Data will be made available on The Bridge of Knowledge.

Declarations

Ethical approval The conducted research is not related to either human or animal use.

Conflict of interest The authors declare that they have no known competing financial interests or personal relationships that could have appeared to influence the work reported in this paper.

Open Access This article is licensed under a Creative Commons Attribution 4.0 International License, which permits use, sharing, adaptation, distribution and reproduction in any medium or format, as long as you give appropriate credit to the original author(s) and the source, provide a link to the Creative Commons licence, and indicate if changes were made. The images or other third party material in this article are included in the article's Creative Commons licence, unless indicated otherwise in a credit line to the material. If material is not included in the article's Creative Commons licence and your intended use is not permitted by statutory regulation or exceeds the permitted use, you will need to obtain permission directly from the copyright holder. To view a copy of this licence, visit <http://creativecommons.org/licenses/by/4.0/>.

References

- Mjos, K.D., Orvig, C.: Metalloids in medicinal inorganic chemistry. *Chem. Rev.* **114**, 4540–4563 (2014). <https://doi.org/10.1021/cr400460s>
- Boechat, N., Kover, W.B., Bastos, M.M., Romeiro, N.C., Silva, A.S., Santos, F.C., Valverde, A.L., Azevedo, M.L., Wollinger, W., Souza, T.M.: Design, synthesis, and biological evaluation of new 3-hydroxy-2-oxo-3-trifluoromethylindole as potential HIV-1 reverse transcriptase inhibitors. *Med. Chem. Res.* **15**, 492–510 (2007). <https://doi.org/10.1007/s00044-007-9004-0>
- Dorozhkin, S.V.: Calcium orthophosphates in nature, biology and medicine. *Materials*. **2**, 399–498 (2009). <https://doi.org/10.3390/ma2020399>
- Yilmaz, B., Alshemary, A.Z., Evis, Z.: Co-doped hydroxyapatites as potential materials for biomedical applications. *Microchem. J.* **144**, 443–453 (2019). <https://doi.org/10.1016/j.microc.2018.10.007>
- Raj, A.K.V., Banerjee, R.H., Sanwal, J., Pathak, N., Chaudhary, N., Arya, A., Sengupta, P.: Ordering of oxygen vacancies in hydroxyapatite under electron irradiation. *Mat. Chem. Phys.* **322**, 129609 (2024). <https://doi.org/10.1016/j.matchemphys.2024.129609>
- Kareem, R.O., Kaygili, O., Ates, T., Bulut, N., Koytepe, S., Kuruçay, A., Ercan, F., Ercan, I.: Experimental and theoretical characterization of Bi-based hydroxyapatites doped with Ce. *Ceram. Int.* **48**, 33440–33454 (2002). <https://doi.org/10.1016/j.ceramint.2022.07.287>
- Kareem, R.O., Bulut, N., Kaygili, O.: Hydroxyapatite biomaterials: A comprehensive review of their properties, structures, medical applications, and fabrication methods. *J. Chem. Rev.* **6**, 1–26 (2024). <https://doi.org/10.48309/jcr.2024.415051.1253>
- Mohammed, B.A., Ates, T., Mahmood, B.K., Kareem, R.O., Keser, S., Bulut, N., Kaygili, O.: The effects of pH on the morphology and structural properties of Er/Yb co-doped hydroxyapatite. *J. Physic Chem. Funct. Mat.* **7**, 11–16 (2024). <https://doi.org/10.54565/jphcfum.1456331>
- Gopi, D., Shinyjoy, E., Kavitha, L.: Synthesis and spectral characterization of silver/magnesium co-substituted hydroxyapatite for biomedical applications. *Spectrochim. Acta Mol. Biomol. Spectrosc.* **127**, 286–291 (2014). <https://doi.org/10.1016/j.saa.2014.02.057>
- Kareem, R.O.: Synthesis and characterization of bismuth-based hydroxyapatites doped with cerium. Master's Thesis, Institute of Science, Firat University, Elazığ/Turkey (2023)
- Korkmaz, A.A., Ahmed, L.O., Kareem, R.O., Kebiroglu, H., Ates, T., Bulut, N., Kaygili, O., Ates, B.: Theoretical and experimental characterization of Sn-based hydroxyapatites doped with Bi. *J. Aust. Ceram. Soc.* **58**, 803–815 (2022). <https://doi.org/10.1007/s41779-022-00730-5>
- Riaz, M., Zia, R., Ijaz, A., Hussain, T., Mohsin, M., Malik, A.: Synthesis of monophasic ag doped hydroxyapatite and evaluation of antibacterial activity. *Mater. Sci. Eng. C.* **90**, 308–313 (2018). <https://doi.org/10.1016/j.msec.2018.04.076>
- Carrera, K., Huerta, V., Orozco, V., Matutes, J., Fernández, P., Graeve, O., Herrera, M.: Formation of vacancy point-defects in hydroxyapatite nanobelts by selective incorporation of Fe³⁺ ions in Ca (II) sites. A CL and XPS study. *Mater. Sci. Eng. B.* **271**, 115308 (2021). <https://doi.org/10.1016/j.mseb.2021.115308>
- Rajendran, A., Barik, R.C., Natarajan, D., Kiran, M., Pattanayak, D.K.: Synthesis, phase stability of hydroxyapatite–silver composite with antimicrobial activity and cytocompatibility. *Ceram. Int.* **40**, 10831–10838 (2014). <https://doi.org/10.1016/j.ceramint.2014.03.075>
- Bulut, N., Kaygili, O., Hssain, A.H., Dorozhkin, S.V., Abdelghani, B., Orek, C., Kebiroglu, H., Ates, T., Kareem, R.O.: Mg-dopant effects on band structures of zn-based hydroxyapatites: A theoretical study. *Iran. J. Sci.* **47**, 1843–1859 (2023). <https://doi.org/10.1016/j.ceramint.2014.03.075>
- Mohammed, B.A., Ates, T., Mahmood, B.K., Kareem, R.O., Keser, S., Bulut, N., Kaygili, O.: Investigation of the effects of glycerol addition as a catalyst on the morphology and structural properties of Gd/Er co-doped hydroxyapatite. *J. Physic Chem. Funct. Mat.* **7**, 28–31 (2024). <https://doi.org/10.54565/jphcfum.1458970>
- Kim, T., Feng, Q.L., Kim, J., Wu, J., Wang, J.H., Chen, G., Cui, F.: Antimicrobial effects of metal ions (Ag⁺, Cu²⁺, Zn²⁺) in hydroxyapatite. *J. Mat. Sci. Mat. Med.* **9**, 129–134 (1998). <https://doi.org/10.1023/A:1008811501734>

18. Lee, J.S.: Silver nanomaterials for the detection of chemical and biological targets. *Nanotechnol. Rev.* **3**, 499–513 (2014). <https://doi.org/10.1515/ntrev-2014-0017>
19. Ciobanu, C.S., Massuyeau, F., Constantin, L.V., Predoi, D.: Structural and physical properties of antibacterial Ag-doped nano-hydroxyapatite synthesized at 100°C. *Nanoscale Res. Lett.* **6**, 1–8 (2011). <https://doi.org/10.1186/1556-276X-6-613>
20. Peetsch, A., Greulich, C., Braun, D., Stroetges, C., Rehage, H., Siebers, B., Köller, M., Epple, M.: Silver-doped calcium phosphate nanoparticles: Synthesis, characterization, and toxic effects toward mammalian and prokaryotic cells. *Colloids Surf. B Biointerfaces.* **102**, 724–729 (2013). <https://doi.org/10.1016/j.colsurf.2012.09.040>
21. Jamuna-Thevi, K., Bakar, S., Ibrahim, S., Shahab, N., Toff, M.: Quantification of silver ion release, in vitro cytotoxicity and antibacterial properties of nanostructured ag doped TiO₂ coatings on stainless steel deposited by RF Magnetron sputtering. *Vacuum.* **86**, 235–241 (2011). <https://doi.org/10.1016/j.vacuum.2011.06.011>
22. Lim, P.N., Teo, E.Y., Ho, B., Tay, B.Y., Thian, E.S.: Effect of silver content on the antibacterial and bioactive properties of silver-substituted hydroxyapatite. *J. Biomed. Mater. Res. A.* **101**, 2456–2464 (2013). <https://doi.org/10.1002/jbm.a.34544>
23. Jacobs, A., Gaulier, M., Duval, A., Renaudin, G.: Silver doping mechanism in bioceramics—from Ag⁺: Doped hap to Ag⁰/BCP nanocomposite. *Crystals.* **9**, 326 (2019). <https://doi.org/10.3390/cryst9070326>
24. Pang, X., Zhitomirsky, I.: Electrodeposition of hydroxyapatite–silver–chitosan nanocomposite coatings. *Surf. Coat. Technol.* **202**, 3815–3821 (2008). <https://doi.org/10.1016/j.surfcoat.2008.01.022>
25. Simon, V., Albon, C., Simon, S.: Silver release from hydroxyapatite self-assembling calcium–phosphate glasses. *J. Non-Cryst Solids.* **354**, 1751–1755 (2008). <https://doi.org/10.1016/j.jnoncrysol.2007.08.063>
26. Bai, X., More, K., Rouleau, C.M., Rabić, A.: Functionally graded hydroxyapatite coatings doped with antibacterial components. *Acta Biomater.* **6**, 2264–2273 (2010). <https://doi.org/10.1016/j.actbio.2009.12.002>
27. Stanić, V., Janačković, D., Dimitrijević, S., Tanasković, S.B., Mitrić, M., Pavlović, M.S., Krstić, A., Jovanović, D., Raičević, S.: Synthesis of antimicrobial monophase silver-doped hydroxyapatite nanopowders for bone tissue engineering. *Appl. Surf. Sci.* **257**, 4510–4518 (2011). <https://doi.org/10.1016/j.apsusc.2010.12.113>
28. Dubnika, A., Loca, D., Salma, I., Reinis, A., Poca, L., Berzina-Cimdina, L.: Evaluation of the physical and antimicrobial properties of silver doped hydroxyapatite depending on the Preparation method. *J. Mat. Sci. Mat. Med.* **25**, 435–444 (2014). <https://doi.org/10.1007/s10856-013-5079-y>
29. Mahanty, A., Shikha, D.: Microstructural, biocompatibility and mechanical investigation of mghap and aghap: Comparative report. *J. Mat. Sci. Mat. Med.* **34**, 22 (2023). <https://doi.org/10.1007/s10856-023-06725-3>
30. Mahanty, A., Kumar, R., Shikha, D.: Enhancement of physiochemical, mechanical, dielectric and antibacterial properties of 10 Wt% PVA-Ag/Mg/Zn doped hydroxyapatite. *Inorg. Chem. Commun.* **163**, 112345 (2024). <https://doi.org/10.1016/j.inoche.2024.112345>
31. Kumar, R., Shikha, D.: Thrombogenicity, DPPH assay, and MTT assay of sol–gel derived 3% silver-doped hydroxyapatite for hard tissue implants. *Int. J. Appl. Ceram. Technol.* **22**, e14884 (2025). <https://doi.org/10.1111/ijac.14884>
32. Shikha, D., Sinha, S.K., Murugesan, S.: Microstructure, corrosion resistance and wettability of hydroxyapatite and silver-doped hydroxyapatite. *J. Surf. Sci. Technol.* **37**, 23–34 (2022). <https://doi.org/10.18311/jsst/2021/26006>
33. Kumar, R., Shikha, D., Sinha, S.K., Guerra-López, J.R., Aboudzadeh, N.: Assessment of antioxidant activity, thrombogenicity and MTT assay of bioceramic phosphate as a biomaterial. *J. Aust Ceram. Soc.* **61**, 333–343 (2025). <https://doi.org/10.1007/s41779-024-01083-x>
34. Kruse, A., Meier, D., Rimbrecht, P., Schacht, M.: Gasification of Pyrocatechol in supercritical water in the presence of potassium hydroxide. *Ind. Eng. Chem. Res.* **39**, 4842–4848 (2000). <https://doi.org/10.1021/ie0001570>
35. Kosobutskii, V.: Pyrocatechol and its derivatives as antioxidants and prooxidants. *Russ J. Gen. Chem.* **84**, 839–842 (2014). <https://doi.org/10.1134/S1070363214050090>
36. Schweigert, N., Zehnder, A.J., Eggen, R.I.: Chemical properties of catechols and their molecular modes of toxic action in cells, from microorganisms to mammals: Minireview. *Environ. Microbiol.* **3**, 81–91 (2001). <https://doi.org/10.1046/j.1462-2920.2001.00176.x>
37. Keser, S., Dogan, A., Ates, T., Barzinjy, A.A., Ates, B., Tekin, S., Sandal, S., Kareem, R.O., Özcan, İ., Bulut, N., Kaygili, O.: Effects of Gallic acid and Quercetin on the structural, thermal, spectroscopic, in vitro biocompatibility and electronic properties of Au-based hydroxyapatite structure. *Mat. Chem. Phys.* **327**, 129892 (2024). <https://doi.org/10.1016/j.matchemphys.2024.129892>
38. Keser, S., Firat, M., Barzinjy, A.A., Kareem, R.O., Ates, T., Ates, B., Tekin, S., Sandal, S., Özcan, İ., Bulut, N., Kaygili, O.: Impact of Quercetin and Gallic acid on the electronic, structural, spectroscopic, thermal properties and in vitro bioactivity of silver-modified hydroxyapatite. *Mat. Chem. Phys.* **339**, 130751 (2025). <https://doi.org/10.1016/j.matchemphys.2025.130751>
39. Cullity, B.D.: Elements of X-ray Diffraction, 2nd Edition, Addison–Wesley Publishing Company, Massachusetts (1987)
40. Landi, E., Tampieri, A., Celotti, G., Sprio, S.: Densification behaviour and mechanisms of synthetic hydroxyapatites. *J. Eur. Ceram. Soc.* **20**, 2377–2387 (2000). [https://doi.org/10.1016/S0955-2219\(00\)00154-0](https://doi.org/10.1016/S0955-2219(00)00154-0)
41. Mabileau, G., Filmon, R., Petrov, P.K., Baslé, M.F., Sabokbar, A., Chappard, D.: Cobalt, chromium and nickel affect hydroxyapatite crystal growth in vitro. *Acta Biomater.* **6**, 1555–1560 (2010). <https://doi.org/10.1016/j.actbio.2009.10.03>
42. Kaygili, O., Keser, S., Dorozhkin, S.V., Yakuphanoglu, F., Al-Ghamdi, A.A., Kirbag, S., Sertkaya, D., Ates, T., Gursoy, N.C.: Structural and dielectrical properties of Ag- and Ba-substituted hydroxyapatites. *J. Inorg. Organomet. Polym. Mater.* **24**, 1001–1008 (2014). <https://doi.org/10.1007/s10904-014-0074-4>
43. Aqib, M., Alomar, M., Anwar, A., Naseem, K., Javaid, A., Intisar, A., Khan, S., Ajaz, H., Khan, I.H.: Synthesis, characterization and antimicrobial analysis of metal-doped (Zn²⁺ and Ag⁺) brushite powder for bone regeneration. *Mat. Chem. Phys.* **320**, 129460 (2024). <https://doi.org/10.1016/j.matchemphys.2024.129460>
44. Makarova, S.V., Borodulina, I.A., Prosanov, I.Y., Borisenko, T.A., Logutenko, O.A., Bulina, N.V., Ishchenko, A.V.: Silver-substituted hydroxyapatite: Mechanochemical synthesis and thermal stability. *Ceram. Int.* **49**, 37957–37966 (2023). <https://doi.org/10.1016/j.ceramint.2023.09.125>
45. Sahin, B., Ates, T., Karaca Acari, I., Barzinjy, A.A., Ates, B., Ozcan, I., Bulut, N., Keser, S., Kaygili, O.: Tuning electronic properties of hydroxyapatite through controlled doping using zinc, silver, and Praseodymium: A density of States and experimental study. *Ceram. Int.* **50**, 7919–7929 (2024). <https://doi.org/10.1016/j.ceramint.2023.12.120>
46. Adhithyan, T., Dhanaraj, K., Gubendhiran, S., Suresh, G., Thenpandiyan, E., Prasath, M.: Green synthesized silver and zinc doped hydroxyapatite photocatalysts to remove methylene blue

- and Rhodamine B dyes from industrial wastewater. *Chem. Phys. Impact.* **9**, 100695 (2024). <https://doi.org/10.1016/j.chphi.2024.100695>
47. Hossain, S., Sarkar, S., Ahmed, S.: Crystallographic characterization of Ag-doping in nanocrystallite hydroxyapatite and evaluation of photocatalytic activity of organic pollutants. *Int. J. Ceramic Eng. Sci.* **7**, e10250 (2025). <https://doi.org/10.1002/ces2.10250>
 48. Méndez-Lozano, N., Apatiga-Castro, M., Ruiz-Baltazar, A.J., Luz-Asunción, M., Pérez-Ramírez, E.E.: Characterization and evaluation of silver concentrations in hydroxyapatite powders. *J. Funct. Biomater.* **14**, 467 (2023). <https://doi.org/10.3390/jfb14090467>
 49. Mansour, S.F., El-Dek, S.I., Ahmed, M.K.: Physico-mechanical and morphological features of zirconia substituted hydroxyapatite nano crystals. *Sci. Rep.* **7**, 1–21 (2017). <https://doi.org/10.1038/srep43202>
 50. Robles-Águila, M.J., Reyes-Avendaño, J.A., Mendoza, M.E.: Structural analysis of metal-doped (Mn, Fe, Co, Ni, Cu, Zn) calcium hydroxyapatite synthesized by a sol-gel microwave-assisted method. *Ceram. Int.* **43**, 12705–12709 (2017). <https://doi.org/10.1016/j.ceramint.2017.06.154>
 51. Koutsopoulos, S.: Synthesis and characterization of hydroxyapatite crystals: A review study on the analytical methods. *J. Biomed. Mater. Res.* **62**, 600–612 (2002). <https://doi.org/10.1002/jbm.10280>
 52. Rajan, K.V.R., Nagesh, S., Mani, S.P.: Preparation, characterization, and assessment of antimicrobial properties of silver-doped hydroxyapatite nanoparticles in orthodontic composite. *J. Adv. Oral Res.* **15**, 179–185 (2024). <https://doi.org/10.1177/23202068241247952>
 53. Lima, J.F.M., Mainardi, M.C.A.J., Rontani, R.M.P., Filho, U.P.R., Liporoni, P.C.S., Calegari, M.L., Rischka, K., Aguiar, F.H.B.: Bioinspired catechol chemistry for dentin remineralization: A new approach for the treatment of dentin hypersensitivity. *Dent. Mater.* **36**, 501–511 (2020). <https://doi.org/10.1016/j.dental.2020.01.012>
 54. Ayhan, Y.M., Ates, T., Seçkin, T., Özcan, I., Bulut, N., Kuruçay, A., Kaygılı, O.: The effects of Zn and Yb co-dopants on the electronic, radiation shielding, structural, thermal and spectroscopic properties of hydroxyapatite. *Chem. Phys. Imp.* **8**, 100488 (2024). <https://doi.org/10.1016/j.chphi.2024.100488>
 55. Ateş, H.G., Kaygılı, O., Bulut, N., Osmanlioğlu, F., Keser, S., Tatar, B., Mahmood, B.K., Ates, T., Ercan, F., Ercan, I., Ates, B., Özcan, I.: Investigation of the structural, thermal, magnetic and cell viability properties of Ce/Sr co-doped hydroxyapatites. *J. Mol. Struct.* **1283**, 135318 (2023). <https://doi.org/10.1016/j.molstruc.2023.135318>
 56. Goldberg, M.A., Protsenko, P.V., Smirnov, V.V., Antonova, O.S., Smirnov, S.V., Kononov, A.A., Vorckachev, K.G., Kudryavtsev, E.A., Barinov, S.M., Komlev, V.S.: The enhancement of hydroxyapatite thermal stability by Al doping. *J. Mater. Res. Technol.* **9**, 76–88 (2020). <https://doi.org/10.1016/j.jmrt.2019.10.032>
 57. Ahmed, L.O., Bulut, N., Osmanlioğlu, F., Tatar, B., Kebiroglu, H., Ates, T., Koytepe, S., Ates, B., Keser, S., Kaygılı, O.: Theoretical and experimental investigation of the effects of Pr Dopant on the electronic band structure, thermal, structural, in vitro biocompatibility of Er-based hydroxyapatites. *J. Mol. Struct.* **1280**, 135095 (2023). <https://doi.org/10.1016/j.molstruc.2023.135095>
 58. Kaygılı, O., Keser, S., Selcuk, A.B., Bulut, N., Koytepe, S., Yahia, I.S., Ates, T.: The effects of gamma irradiation on dielectric properties of Ag/Gd co-doped hydroxyapatites. *J. Mater. Sci. Mater. Electron.* **30**, 10443–10453 (2019). <https://doi.org/10.1007/s10854-019-01387-w>
 59. Dorozhkin, S.V.: Bioceramics of calcium orthophosphates. *Biomaterials.* **31**, 1465–1485 (2010). <https://doi.org/10.1016/j.biomaterials.2009.11.050>

Publisher's note Springer Nature remains neutral with regard to jurisdictional claims in published maps and institutional affiliations.